THE JOURNAL OF PHYSICAL CHEMISTRY C

Article

pubs.acs.org/JPCC

Computational Study of Al and Sc NMR Shielding in Metallic ScTT′Al Heusler Phases

Khoong Hong Khoo,[†] Robert Laskowski,*[,†] and Peter Blaha[‡]

[†]Institute of High Performance Computing, A*STAR, 1 Fusionopolis Way, #16-16, Connexis, Singapore 138632

[‡]Institute of Materials Chemistry, Vienna University of Technology, Getreidemarkt 9/165-TC, A-1060 Vienna, Austria

ABSTRACT: The results of first-principles calculations of Al and Sc NMR shielding for a set of ScTT′Al Heusler phase compounds are reported and compared to recently published experimental NMR shifts. The orbital component of the shielding (chemical shift) is computed using density functional perturbation formalism. The spin part (Knight shift) is evaluated using a direct self-consistent approach, where a finite external magnetic field acting on the electron spin is added to the density functional theory (DFT) Hamiltonian. Both approaches are implemented in the full potential linearized augmented plane wave method. We show that, for Al, the calculated and measured shifts match quite well except for the ScNiAuAl case, which is probably due to an experimental problem as the reported lattice parameter is also unrealistic. For Sc nuclei, we find three such unmatched cases between theory and experiment and we discuss possible sources of this discrepancy. For selected compounds, the effects of composition and lattice size on the computed shielding are determined. In addition, we performed a detailed analysis of the paramagnetic and diamagnetic components of the Knight shift. Most notably, the Knight shift is found to be fairly "unimportant" for Sc shieldings as the large valence and core contributions cancel each other and the large variations in the shifts originate solely from orbital contributions, a quantity usually assumed to be constant in metallic systems. Finally, we compare our results with recently published data for Al shielding in ScT_2Al obtained using a plane-wave pseudopotential based method.

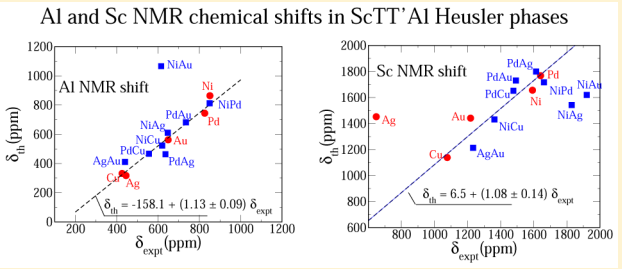

INTRODUCTION

Density functional theory[1,2] (DFT) calculations of nuclear magnetic resonance (NMR) shielding in solids present in principle a relatively straightforward way to aid the interpretation of measured spectra. In the case of insulating solids, where only the response of orbital motion contributes to the screening of the external magnetic field, the approach is well-established and has been used for years.[3,4] The situation is much more complicated for metallic systems, where the interaction of the external field with the spin of the electrons leads to repopulation of electronic states around the Fermi level, resulting in a spin current that contributes directly to the screening. The resulting spin density modifies the existing potential and polarizes the lower (core) eigenstates, constituting a source of technical difficulties that may lead to potential issues. For these reasons, there are only very few reported studies of NMR calculations in metals.[5−7] However, these studies also show that carefully approaching such problems can result in reliable computed NMR shieldings.

In order to expand the application base of our recently published computational scheme for calculating NMR shielding in metals,[5] we report on the isotropic shielding at Sc and Al sites in Heusler phases with general composition ScTT′Al, where T and T′ are transition metals. We compare our results to recently published experimental data.[8] The availability of experimental NMR data presents a valuable opportunity for studying the relation between NMR parameters and the atomic and electronic structures as well as the specific material composition, since this is in general not very well understood in solids. The NMR shielding at the Al site has been recently computed by another group using a similar approach but with a different DFT code.[7] Unfortunately, these authors did not present their results for Sc shieldings; however, a comparison of Al shieldings from these two approaches is still valuable for the validation of computational methodologies.

The Heusler phases XTT′Y are cubic compounds spanning a wide range of chemical compositions. They exhibit several physical properties[9] such as magnetic phases,[10] giant magnetoresistance,[11] enhanced thermoelectricity,[12] and superconductivity[13] that may be considered as technologically relevant. In a recent study, the ternary compounds ScT_2Al, where T = Ni, Pd, Cu, Ag, Au, and quaternary compounds ScTT′Al, with TT′ = NiCu, NiAg, PdCu, NiPd, NiAu, PdAu, and AgAu, have been synthesized and their NMR chemical shieldings were reported.[8] Powder X-ray diffraction measurements have shown that the ternary ScT_2Al Heusler alloys crystallize in the cubic $MnCu_2Al$-type structure ($Fm\bar{3}m$), where the Al and Sc atoms are arranged in an NaCl fashion and the T atoms are placed inside the voids of the Sc−Al sublattice such that each Sc/Al atom is surrounded by eight transition metal atoms arranged in the

Received: April 13, 2017
Revised: May 19, 2017
Published: May 19, 2017

DOI: 10.1021/acs.jpcc.7b03494
J. Phys. Chem. C 2017, 121, 12398−12406

shape of a cube (Figure 1). For the quaternary compounds ScTT′Al, there are two structures being considered: $MnCu_2Al$

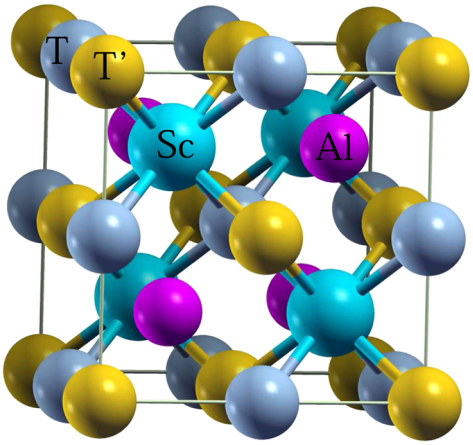

Figure 1. Atomic structure of ScTT′Al, where T, T′ = Ni, Pd, Cu, Ag, Au. For the quaternary cases of T ≠ T′ the structure is of LiMgPdSn type ($F4\bar{3}m$) with two distinct transition metal sites. For the special case of T = T′, we recover the $MnCu_2Al$-type structure ($Fm\bar{3}m$).

($Fm\bar{3}m$) with one mixed occupied transition metal site (disordered) and LiMgPdSn ($F4\bar{3}m$) with two distinct transition metal sites (ordered). Single crystal diffraction measurements have suggested that the $MnCu_2Al$ ($Fm\bar{3}m$) structure is more favorable, but we pick the LiMgPdSn ($F4\bar{3}m$) structure for ease of computation, and we will show that the exact ordering of the T and T′ atoms do not considerably affect the NMR shielding. All our results have been obtained with experimental lattice parameters provided in ref 8, even though we found the ScNiAuAl value to be possibly incorrect (see below).

DETAILS OF THE COMPUTATIONAL APPROACH

Two main contributions to the NMR shift in the measured spectra have to be considered. These are the chemical shift (δ_{orb}) resulting from the orbital motions of the electrons (we will refer to this as the orbital component) and the Knight shift ($\mathcal{K}$)[14−17] (also called the spin component). The latter is due to the interaction of the nuclear magnetic moment with the spins of the electrons in metallic materials. However, $\mathcal{K}$ and δ_{orb} cannot be separated experimentally and the complete isotropic signal shift δ_{iso} in metallic materials is given by[18]

$$\delta_{iso} = \delta_{orb} + \mathcal{K} \tag{1}$$

From the computational point of view, the NMR shielding $\vec{\sigma}$ tensor describes the response of a system to an external magnetic field. It is defined as a proportionality between the induced magnetic field $\mathbf{B}_{ind}$ at the nucleus at site $\mathbf{R}$ and the external uniform field $\mathbf{B}$:

$$\mathbf{B}_{ind}(\mathbf{R}) = -\vec{\sigma}(\mathbf{R})\mathbf{B} \tag{2}$$

We focus our discussion on the isotropic component, defined by

$$\sigma_{iso}(\mathbf{R}) = \mathrm{Tr}[\vec{\sigma}(\mathbf{R})] \tag{3}$$

and we drop the subscript "iso" for simplicity. The shielding can be measured only with respect to a reference compound, and as a result we introduce the isotropic shift as

$$\delta_{iso}(\mathbf{R}) = \sigma_{ref} - \sigma_{iso}(\mathbf{R}) \tag{4}$$

The external magnetic field is a relatively weak perturbation compared to the typical energy scale of the electronic structure; therefore, its effect on the spin and orbital motion of an electron can be separated in theoretical calculations. The orbital part of the shielding, i.e. the orbital component of the induced field $\mathbf{B}_{ind}$, responsible for the chemical shift is obtained directly from the Biot−Savart law (in atomic units, with c as the speed of light):

$$\mathbf{B}_{ind}(\mathbf{R}) = \frac{1}{c}\int d^3r\,\mathbf{j}(\mathbf{r}) \times \frac{\mathbf{R}-\mathbf{r}}{|\mathbf{r}-\mathbf{R}|^3} \tag{5}$$

where $\mathbf{j}(\mathbf{r})$ is the orbital contribution to the induced current. The method for computing $\mathbf{j}(\mathbf{r})$ is based on a linear response approach[3,4,19] originally developed by Mauri, Pfrommer, and Louie (MPL).[3] It has been adapted and implemented within the all-electron, full potential augmented plane wave (APW) WIEN2k code.[20,21] The details of the implementation are described in our previous publications.[22,23] Formally our approach belongs to a set of gauge transformation methods, often referred to as IGCV (individual gauge for core and valence) with a "$d(r) = r$" gauge choice for the valence electrons.[24]

In order to compute the induced spin density and the spin part of the NMR shielding related to the Knight shift ($\mathcal{K}$), we use a direct approach.[5] We perform self-consistent spin-polarized calculations with a finite external magnetic field (B_{ext}) acting on the electron spin only. The interaction with the external field can be cast into a spin-dependent potential leading to a spin-splitting of eigenstates and a finite spin magnetization. It does not break the translational symmetry of the solid, and therefore such calculations are in principle straightforward. The induced magnetic field at a given nucleus is computed using an expression for the magnetic hyperfine field:[25]

$$B_{hf} = \frac{8\pi}{3}\mathbf{m}_{av} + \int \frac{S(r)}{r^3}[3(\mathbf{m}(r)\hat{r})\hat{r} - \mathbf{m}(r)] \tag{6}$$

where the first term is the Fermi contact term (B_c), and the second captures the spin-dipolar contribution (B_{sd}) to the hyperfine field. The spin contribution (σ_s), e.g. the Knight shift ($\mathcal{K}$) to the shielding is then simply given by two terms:

$$\sigma_s = \sigma_c + \sigma_{sd} = -B_c/B_{ext} - B_{sd}/B_{ext} \tag{7}$$

The Fermi contact term (σ_c) is related to the average spin density ($m_{av}(r) = \rho_{up}(r) - \rho_{dn}(r)$) within the Thomson radius around the nucleus.[25] For the systems studied in this work the spin-dipolar contribution vanishes due to the symmetry of the lattice. Further details and benchmarks of our approach can be found in ref 5. In order to obtain a sizable response and evaluate the NMR shielding with a numerical precision at the level of 1 ppm, we apply in our calculations a field B_{ext} of 100 T, which induces a spin-splitting of approximately 1 mRy. We have checked the linearity of the induced field with respect to the external field. This scheme presents an alternative approach to the linear response formalism proposed in ref 26. However, our scheme allows the capture of effects that appear only when the magnetic response is evaluated self-consistently. As we will show later, these self-consistency effects are of particular importance for elements with valence d-electrons.

The NMR calculations within our APW method do not require any computational parameters considerably different

DOI: 10.1021/acs.jpcc.7b03494
J. Phys. Chem. C 2017, 121, 12398−12406

Table 1. Calculated and Experimental[8] Al and Sc NMR Shifts (δ and δ_{exp} in ppm) in ScT_2Al and $ScTT'Al$ and the Decomposition of the NMR Shielding into Orbital (σ_o) and Spin (σ_s) Components[a]

T/TT′	δ	δ_{exp}	σ_o	σ_s	σ_s^{core}	σ_s^{val}	σ_s^{para}	σ_s^{dia}	σ_s^{SCF}	$\sigma_s^{val-SCF}$
				Al						
Ni	868	851	312 (2.9)	−619 (1.5)	10	−629	−415	27	−231	−241
Pd	748	826	347 (2.1)	−534 (0.0)	13	−547	−472	31	−93	−106
Cu	336	426	270 (15.3)	−45 (2.5)	15	−60	−173	26	102	87
Ag	322	445	298 (15.2)	−59 (2.5)	13	−72	−225	34	132	119
Au	566	649	460 (11.8)	−465 (7.5)	17	−482	−456	35	−44	−61
Pt	1148		384 (3.3)	−971 (3.0)	5	−976	−780	32	−223	−228
NiCu	526	620	365 (2.6)	−331 (1.5)	17	−348	−310	26	−47	−64
NiAg	615	647	367 (3.1)	−421 (2.0)	17	−438	−381	29	−69	−86
NiAu	1070	615	383 (1.7)	−892 (6.5)	11	−903	−625	28	−295	−306
PdCu	471	556	384 (1.9)	−294 (2.0)	17	−311	−337	26	17	0
PdAg	468	636	395 (3.0)	−302 (2.5)	18	−320	−358	32	24	6
PdAu	686	735	417 (1.9)	−542 (2.5)	14	−556	−498	32	−76	−90
AgAu	415	440	319 (19.9)	−173 (3.0)	15	−188	−242	31	38	23
NiPd	816	850	333 (3.4)	−588 (0.5)	12	−600	−450	29	−167	−179
				Sc						
Ni	1658	1592	−868 (9.9)	15 (9.0)	220	−205	−270	23	262	42
Pd	1770	1641	−846 (5.8)	−119 (1.0)	430	−549	−255	24	112	−318
Cu	1141	1077	−324 (29.1)	−12 (3.5)	493	−505	−190	22	156	−337
Ag	1454	648	−724 (28.9)	74 (6.5)	652	−578	−188	25	237	−415
Au	1443	1218	−592 (29.3)	−47 (13.5)	661	−708	−296	24	225	−436
Pt	1745		−755 (19.6)	−186 (3.5)	284	−470	−301	26	89	−195
NiCu	1433	1362	−783 (5.4)	154 (1.5)	532	−378	−191	24	321	−211
NiAg	1544	1829	−1041 (14.5)	302 (0.0)	651	−349	−183	21	464	−187
NiAu	1621	1920	−895 (8.7)	78 (6.0)	523	−445	−299	25	352	−171
PdCu	1654	1477	−889 (8.8)	40 (0.5)	624	−584	−181	25	196	−428
PdAg	1802	1614	−1104 (14.1)	107 (0.5)	696	−589	−160	25	242	−454
PdAu	1732	1492	−889 (12.7)	−39 (0.5)	539	−578	−233	24	170	−369
AgAu	1215	1233	−473 (36.4)	62 (4.0)	538	−476	−165	25	202	−336
NiPd	1719	1661	−850 (4.7)	−64 (3.5)	321	−385	−264	26	174	−147

[a]The numbers in parentheses represent the slope: $[\sigma(2\ \text{mRy}) - \sigma(4\ \text{mRy})]/2$ mRy, where $\sigma(T)$ is the shielding computed with Fermi temperature T. σ_s is decomposed into core (Al 1s2s2p, Sc 1s2s2p3s3p) σ_s^{core} and valence σ_s^{val} contributions. σ_s^{para} and σ_s^{dia} show the non-self-consistent paramagnetic and diamagnetic contributions to σ_s (see text for details), σ_s^{SCF} ($\sigma_s^{val-SCF}$) captures the effect of the total (valence) self-consistent spin response to the external magnetic field. The calculated shielding for the reference compounds $AlPO_4$ and $ScPO_4$ are 515.6 and 847.5 ppm, respectively, and the corresponding measured shifts are equal to 45[26] and −42.6 ppm.[28] Thus, the theoretical shielding is related to the theoretical shifts by δ = 847.5 (515.6) − 42.6 (+ 45) − σ for Sc (Al).

from generally accepted defaults, except the Brillouin zone (BZ) sampling. For the sake of analysis we keep the atomic sphere radii for Al and Sc atoms constant at 2.3 and 2.4 au, respectively. The plane wave cutoff K_{max} for the APW basis set is determined by RK_{max} = 8.0, where R represents the smallest atomic radius in a calculation. The calculations have been carried out with the Perdew, Burke, Ernzerhof (PBE)[27] version of the generalized gradient approximation (GGA) to the DFT exchange−correlation functional. The Brillouin zone was sampled with a regular mesh of 50 × 50 × 50 k-points for both the spin and orbital components of the NMR shielding. In order to accelerate the convergence of the calculated shieldings with respect to the density of the BZ sampling, the occupancies of the electronic states are "smeared" out around the Fermi level[5] with a Fermi−Dirac function. We noticed[5,6] that in some cases the applied "smearing" affects the computed NMR shielding. Therefore, we consider it necessary to estimate this effect. As in our previous publications[5,6] we calculate the slope describing the dependence of the shielding on the "smearing" temperature by finite differences: $[\sigma(T_1) - \sigma(T_2)]/(T_2 - T_1)$, where $\sigma(T)$ is the shielding computed with temperature T; in this work T_1 and T_2 are set to 2 and 4 mRy, respectively. Note that 2 mRy corresponds roughly to room temperature.

The measured NMR shifts[8] have been referenced to 1 M $Al(NO_3)_3$ and 0.1 M $Sc(NO_3)_3$ solutions for Al and Sc, respectively. Since we cannot compute the shifts of such solutions, we used instead $AlPO_4$ and $ScPO_4$ as intermediate references. Known experimental values of Al and Sc shifts in $AlPO_4$ and $ScPO_4$ allow us to deduce the appropriate reference and estimate theoretical values of NMR shifts. The experimental NMR shift[28] at Sc in $ScPO_4$ is equal to −42.6 ppm; however, it is referenced with respect to an aqueous $ScCl_3$ solution instead of $Sc(NO_3)_3$. For $AlPO_4$, the measured value of 45 ppm has been obtained with respect to a solution of $AlCl_3$ in heavy water. This reference was used in earlier DFT calculations[5,26] for pure Al. Considering the highly ionic nature of all these references, the discrepancy caused by using inconsistent references should be rather marginal and not affect our conclusions.

RESULTS AND DISCUSSION

The results of our calculations are summarized in Table 1. The effect of thermal smearing is larger for the orbital part of the

DOI: 10.1021/acs.jpcc.7b03494
J. Phys. Chem. C 2017, 121, 12398−12406

shielding than for the spin component, and more sizable for Sc than for Al results. Besides, the eventual corrections to the calculated shielding due to the finite smearing definitely do not affect our discussion.

The direct comparison between computed and measured[8] shifts is presented in Figure 2. For Al shifts in Figure 2a, the

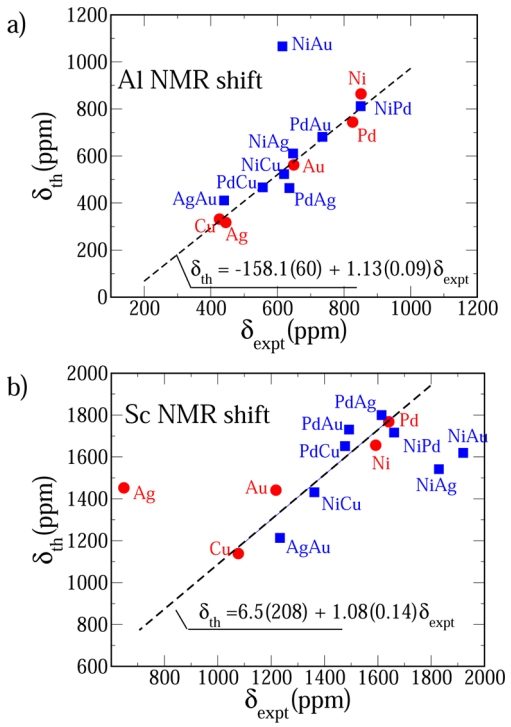

Figure 2. Correlation of computed and measured NMR shifts for (a) Al and (b) Sc in ScT_2Al (dots) and ScTT′Al (squares). The measured NMR shifts are taken from ref 8.

correlation is very good excluding the data point corresponding to ScNiAuAl. The slope of the relation is close to 1.0, and the free coefficient is reasonably close to zero. The Al shift for ScNiAuAl in Figure 2a has been calculated using the experimental lattice parameter a_{NiAu} = 6.7183 Å taken from ref 8. This number, however, is clearly beyond the expected range that may be deduced from the lattice sizes of $ScNi_2Al$ (a_{Ni} = 5.990 Å) and $ScAu_2Al$ (a_{Au} = 6.5329 Å). Total energy calculations fully confirm Vegard's law, by which a_{NiAu} is close to an average of a_{Ni} and a_{Au}. This indicates that, for this particular case, the problem may be due to "suspicious" lattice parameters reported in ref 8, or even a "suspicious" sample. The effect of the lattice parameter on Al and Sc shifts in ScNiAuAl is shown in Figure 3. For Al, the total shift increases when the lattice is expanded, mainly due to its spin part. As a result, using the average $(a_{Ni} + a_{Au})/2$ value as the lattice parameter instead of the experimental a_{NiAu} makes the Al shift appear closer to the correlation line by about 300 ppm, while a correction close to 500 ppm is required for a perfect fit in Figure 2a.

The theoretical and experimental Sc shifts shown in Figure 2b are more scattered than for Al, but if we exclude the Ag and NiAu cases, a linear fit leads to a nice correlation with a slope of 1.08. The larger discrepancies for Sc shifts relative to Al may be attributed to its more localized valence states (Sc 3d versus Al 3p). Still, there are several other compounds, in particular the quaternary ones, that deviate a bit from the ideal correlation line. Obvious guesses for possible sources of discrepancy are

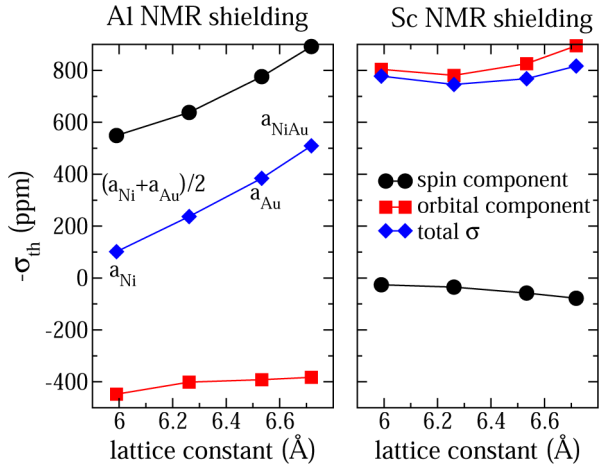

Figure 3. Dependence of computed Al (left) and Sc (right) NMR shielding in ScNiAuAl on the lattice constant. Besides the total shielding (diamonds), we also show orbital (squares) and spin (dots) contributions to the shielding. Different data points for the same concentration represent different atomic arrangements in the 4 times larger supercell.

the use of wrong lattice parameters and the use of perfectly ordered, idealized structural models for the ternary alloys. However, as we see in Figure 3, the dependency of the Sc shielding on the lattice parameter is much weaker than for Al, and ScNiAuAl is one of the "bad" points in Figure 2b. Besides the lattice parameter, variations of composition and various possible arrangements of T and T′ atoms may also impact the agreement between the calculated and measured data for quaternary compounds. As an example, we present in Figure 4

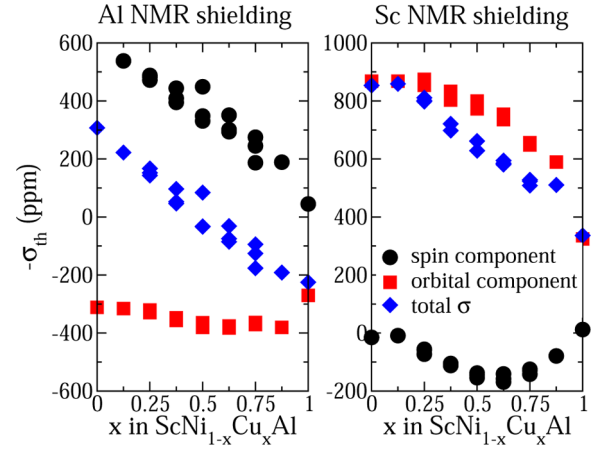

Figure 4. Dependence of computed Al (left) and Sc (right) NMR shielding on the composition in $ScNi_{1-x}Cu_xAl$. We show total shielding (diamonds), as well as spin (dots) and orbital (squares) components.

the dependence of the calculated shielding on the composition for $ScNi_{1-x}Cu_xAl$. The multiple data points for a given x show the variation due to different ordering of T and T′ metal atoms in a primitive supercell that is 4 times larger than the ordered ($F\bar{4}3m$) unit cell. For this example, the variation of the total shielding with x for both Al and Sc is quite monotonic. For Al, the variations of shielding due to ordering do not exceed 100 ppm for x around 0.5. The orbital component does not change with x, and the trend is determined by the spin contribution. Sc

DOI: 10.1021/acs.jpcc.7b03494
J. Phys. Chem. C 2017, 121, 12398−12406

shows an opposite relation, with a nonmonotonic dependence of the spin component on x. As a conclusion, we did not find clear evidence to attribute the weak correlation between theory and experiment to the atomic structure, although one would need to consider every specific case in detail, both in experiment and in theory, to know for sure.

The induced spin-dependent potentials and densities in Figure 5 show that Al and Sc atoms respond differently to the

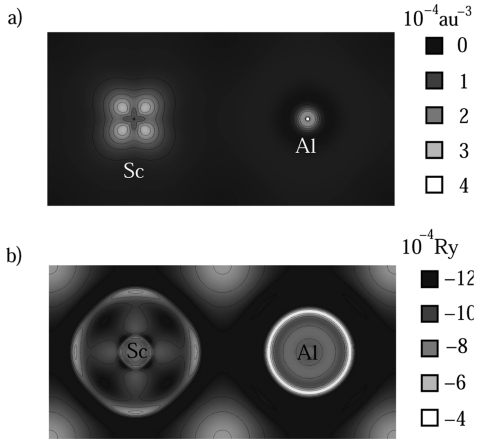

Figure 5. (a) Self-consistent spin density in the presence of an external magnetic field of 100 T computed for ScNiAuAl. (b) Difference between self-consistent spin up and spin down potentials in ScNiAuAl in the presence of an external magnetic field of 100 T. The magnetic field of 100 T corresponds to the uniform potential difference of 8.5×10^{-4} Ry.

external magnetic field. Due to the Sc 3d valence electrons, both spin density and potential induced around Sc have a more complicated shape indicating a fairly localized induced Sc 3d moment of t_{2g} symmetry. Obviously, due to the given point group, the induced spin density (potential) around Al, which originates from s and p electrons, must be spherical. In this context, Sc can be more challenging for theoretical calculations than Al, especially when considering the self-consistent component of the spin part of the shielding and the well-known fact that particular GGA functionals tend to overestimate magnetic effects in some transition metal compounds.[29,30]

We also believe that there are no problems in obtaining accurate values for the orbital part of the Sc NMR shifts with our calculations. For instance, the orbital shieldings for a series of insulating Sc compounds given in Table 2 and Figure 6 are in excellent agreement with experiment.[28] The theory vs experiment correlation in Figure 6 shows discrepancies not exceeding a few parts per million.

For the orbital part of the shielding, core and semicore states (not shown in Table 1) always give a positive (diamagnetic) contribution to the NMR shielding that is not sensitive to the atomic environment. The Al 1s2s deep core states and the 2p semicore contribute 531.6 and 232.7 ppm respectively, which sum to 764.3 ppm. For Sc, the 1s2s2p deep core states give 1337.9 ppm, while the 3s3p semicore contributes 162.8 ppm, summing to 1500.7 ppm. For comparison, the total shielding for isolated Al and Sc atoms is 792.7 and 1535.1 ppm, respectively. Thus, the Al 3s3p and Sc 4s3d valence states contribute in the free atom only about 30 ppm to σ_o. In contrast, in our compounds the valence states contribute much more and show a high sensitivity to the specific composition.

Table 2. Calculated Orbital (σ_o), Spin (σ_s), and Total (σ) Shielding for a Series of Insulating Scandium Compounds[a]

			σ_o	σ_s	σ	δ_{exp}
$ScPO_4$	$I4_1/amd$	4a	836	12	848	−42.6
Sc_2O_3	$Ia\bar{3}$	8b	692	8	700	113
		24d	671	8	679	136
ScOF	$P2_1/c$	4e	735	7	742	64
$ScLi_3B_2O_6$	$P2_1/n$	2a	680	10	690	100
Sc_2CaO_4	$Ia\bar{3}$	4c	641	8	649	158
		4c	633	8	641	160

[a]Measured shifts (δ_{exp}) are taken from ref 28.

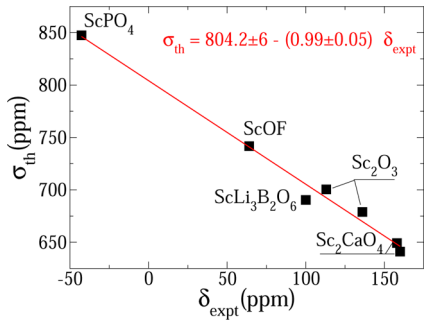

Figure 6. Correlation of theoretical shielding (σ_{th}) and measured Sc shifts (δ_{expt}) for some insulating Sc compounds. Values of δ_{expt} are taken from ref 28.

The orbital component of the Al shielding varies between 300 and 460 ppm, while for Sc this variation is even larger but of opposite sign and lies between −300 and −1100 ppm. If we take away the constant core/semicore contributions, the effect of the valence states is estimated to about −400 ppm for Al 3s3p, and as much as −2500 ppm for Sc 4s3d. The differences between Al and Sc are to be expected, as the Al 3s3p states are considerably more spherical and have no d electrons, in contrast to Sc 4s3d which can produce a much larger induced orbital momentum. The variation of the orbital component within the series of compounds can be understood by performing an analysis based on the character/orbital decomposition as presented in our previous studies for fluorides[31] and sulfides.[32] The variation of the orbital contribution to the shielding is determined by two factors: a direct charge transfer and/or a hybridization between Al/Sc wave functions with the neighboring transition metal valence states, and the details of the electronic structure of the corresponding transition metal neighbor. In view of our previous analysis,[32] it is to be expected that the availability of unoccupied d-states close to the Fermi energy (E_F) leads to a larger paramagnetic contribution. This is in fact the case for the Sc shielding, and in compounds containing T/T′ metals with a partially filled d shell (such as Ni, Pd, Pt), the deshielding effect is much stronger than for those with a full d shell (Cu, Ag, Au).

In order to emphasize the importance of the orbital contribution σ_o to the total magnetic shielding in metals, it is instructive to compare the experimental Sc shifts δ_{exp} for the insulators (see Table 2) with those of the intermetallic compounds (Table 1). We see an average difference of about 1500 ppm which comes almost entirely from the orbital part. The Sc σ_o changes from +700 ppm in insulators to −800 ppm in the metals, while the spin contribution σ_s, even in the metallic compounds, is only on the order of 100 ppm. We want to stress explicitly that the often-assumed correlation between

DOI: 10.1021/acs.jpcc.7b03494
J. Phys. Chem. C 2017, 121, 12398−12406

the paramagnetic shift in metals and their spin contribution (Knight shift) is not at all true for the Sc shifts, but the change is almost solely due to a change of σ_o. This statement is probably true for many other transition metals, and it is only for simple sp-atoms (such as Al) that the Knight shift dominates the total shift in metallic systems.

In order to understand the reason for the surprisingly small σ_s of Sc but the large σ_s for Al, let us look at the decomposition of the spin contribution into the core (σ_s^{core}) and valence (σ_s^{val}) contributions:

$$\sigma_s = \sigma_s^{core} + \sigma_s^{val} \quad (8)$$

Inspection of Table 1 shows that σ_s^{core} for Al (coming from 1s, 2s, 2p states) is extremely small, while for Sc, both σ_s^{core} (originating from 1s, 2s, 2p, 3s, 3p orbitals) and σ_s^{val} have large magnitudes. However, due to their opposite signs, they cancel to a large extent, leading to the small σ_s for Sc. While the orbital part of the shielding can be quite precisely computed within a linear response formalism, this is not true for the spin component, which determines the Knight shift. The way spin degrees of freedom respond to the external magnetic field is more complicated, and self-consistent evaluation of this response is essential. The large core component is a good example of this. The direct effect of the external magnetic field leading to small contraction or expansion of majority or minority spins results in contributions of only a few parts per million. We have included in Table 1 additional columns that capture such self-consistency effects. The numbers under σ_s^{para} represent the paramagnetic contribution to the shielding using a perturbative approach. The procedure to calculate this contribution starts with self-consistent converged charge densities and potentials obtained without the external magnetic field. We then add to the Hamiltonian the external magnetic field acting only on the spin and compute the wave functions and corresponding spin density. The spin density and what follows σ_s^{para} originate in this case from the different occupations of the rigidly shifted spin up and spin down states. In Table 1, the column labeled σ_s^{dia} lists the diamagnetic part of the non-self-consistent response, which is due to the first-order change in the shape of the wave functions. As mentioned before, the spin up and spin down states shift in energy in opposite directions under the influence of the magnetic field. The shape of the wave function depends on its eigenvalue leading to slight contractions and expansions in the spin up and spin down wave functions. Due to these changes, a nonzero spin magnetization at the nucleus appears and contributes to the shielding. In order to evaluate this effect, we start as before from the self-consistent charge density and potential without the external magnetic field. After that, we add to the Hamiltonian the external magnetic field acting only on the spin and compute the charge and spin densities in a similar way to σ_s^{para}, but now we constrain the occupations and force the total magnetization to be zero. We note that such effects should also be present in insulating materials where occupations do not change due to the finite band gap. As we can see in Table 1, this contribution is quite small, with values reaching 20−30 ppm.

In order to capture the self-consistent response to the external magnetic field, we define σ_s^{SCF} as the difference:

$$\sigma_s^{SCF} = \sigma_s - (\sigma_s^{para} + \sigma_s^{dia}) \quad (9)$$

The induced spin magnetization, which is the source of σ_s^{para}, is quite large and it considerably modifies the existing potentials for the spin up and down states. As a result, a self-consistent procedure is needed to properly compute the shielding. Fully converged spin densities and the difference between spin up and spin down potentials are shown for ScNiAuAl in Figure 5. The overall effect represented by σ_s^{SCF} is always positive for Sc; i.e. it tends to cancel paramagnetic contributions. For Al, the sign varies within the series of compounds. We again decompose σ_s^{SCF} into its core σ_s^{core} and valence $\sigma_s^{val-SCF}$ contributions (Table 1). The non-self-consistent core contributions to both Al and Sc shielding is just 20−30 ppm. However, self-consistency leads to large contributions from these states for the case of Sc, with σ_s^{core} varying by as much as 200−700 ppm (Table 1). On the other hand, σ_s^{core} for Al does not change much and remains between 10 and 20 ppm. The variation within the series for Sc shows that any approximations concerning the potential applied to core states need careful consideration.

The total NMR shielding/shifts in metallic compounds are often analyzed or interpreted in terms of the s-orbital projected density of states (s-PDOS) registered at the Fermi level. In principle, only the spin contribution to the shielding σ_s or, strictly speaking, its paramagnetic component σ_s^{para} computed in the way we have done for Table 1 is expected to scale with the value of s-PDOS, especially for cases when the orbital part varies significantly within the analyzed series of compounds. The relation for σ_s and σ_s^{para} are presented in Figure 7. The non-

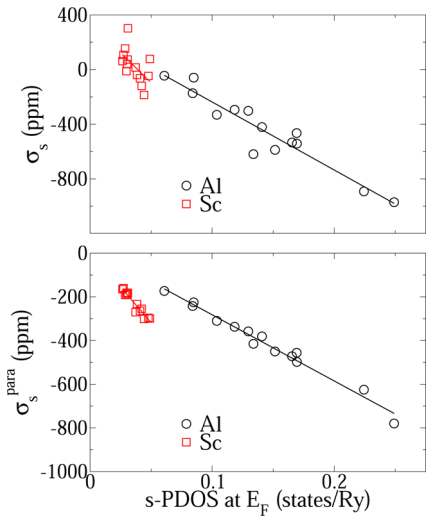

Figure 7. Correlation of the total spin component σ_s (top) and the paramagnetic part σ_s^{para} (bottom) with the s-PDOS at the Fermi level. The procedure used for computing σ_s^{para} is described in the text.

self-consistent σ_s^{para} shows a very nice linear relation with the s-PDOS, while much larger deviations, in particular for Sc, can be found for σ_s. Apparently, σ_s^{SCF} (self-consistent component of σ_s) and the s-PDOS do not correlate with each other.

Let us decompose now σ_s^{SCF} into core (σ_s^{core}) and valence ($\sigma_s^{val-SCF}$) contributions (Table 1):

$$\sigma_s^{SCF} = \sigma_s^{core} + \sigma_s^{val-SCF} \quad (10)$$

As discussed before, the core and semicore contribution to the shielding (σ_s^{core} in Table 1) is entirely an effect of self-consistency. For Sc we can correlate it very nicely with the induced magnetic moments of the corresponding Sc atom (Figure 8b), or, equivalently, with the Sc d-PDOS at the Fermi level, as presented in Figure 8a. In order to rationalize this, we

DOI: 10.1021/acs.jpcc.7b03494
J. Phys. Chem. C 2017, 121, 12398−12406

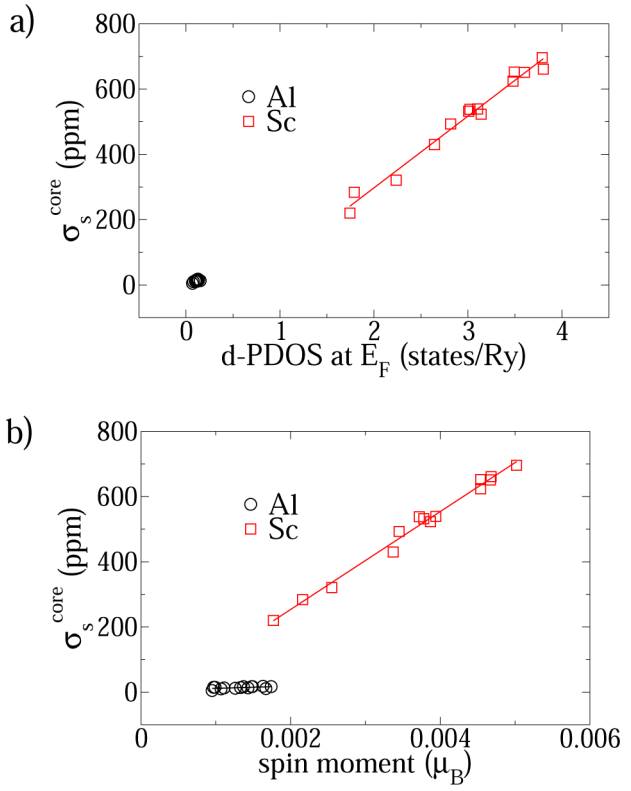

Figure 8. Correlation of core + semicore contributions to spin shielding σ_s^{core} with the value of d-Al/Sc-PDOS at the Fermi level (a) and with the induced spin moment (b) (for 100 T external magnetic field).

notice that the d-PDOS at E_F is proportional to the induced 3d magnetic moment of Sc and this "localized" moment produces a potential shift of opposite sign for all "localized" core and in particular the semicore 3s states of Sc. Since the latter are spatially close to the 3d electrons, they experience the largest effect. Such effects have been documented in studies of ferromagnetic Fe compounds by Mössbauer spectroscopy,[33] where it is often possible to deduce from the measured hyperfine field the total 3d moment of Fe. These hyperfine fields are dominated by core or semicore electrons and have opposite sign compared to the 3d spin polarization. For Al, σ_s^{core} is much smaller because the induced magnetic moments are much smaller and the delocalized character of the Al 3p moments hardly affects the localized Al 1s, 2s core states (Figure 8).

For the valence part of σ_s^{SCF} ($\sigma_s^{val-SCF}$), as demonstrated for Sc in Figure 9, we can identify mainly two contributions. The first one is an on-site effect due to the induced local magnetic moment M^{Sc} (dominated by Sc 3d states), which affects also the valence Sc 4s spin polarization and gives a very nice linear correlation in all compounds except when Ni is present as nearest neighbor. The second effect comes from the fact that the neighboring atoms possess an induced local magnetic moment which induces a transferred hyperfine field at the Sc nucleus. The effect is again well-known in Mössbauer spectroscopy.[34] When these local moments around Sc are similar in magnitude, they contribute to a more or less constant shielding and one does not need to consider them explicitly. However, the induced magnetic moments for Ni (0.008−0.013 μ_B/100T) are typically 3−10 times bigger than those of other transition metals in this study (0.001−0.003 μ_B/100T).

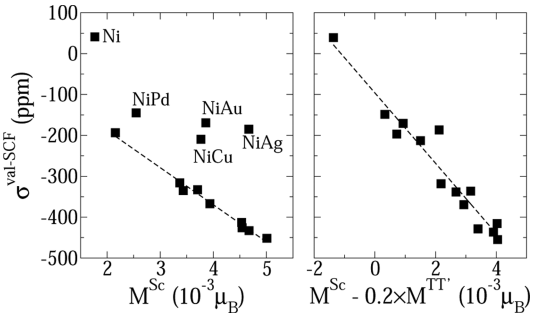

Figure 9. Dependency of Sc $\sigma_s^{val-SCF}$ on the induced Sc magnetic moment M^{Sc} (left) or the combined effective moment (M^{Sc} − 0.2 $M^{TT'}$), where $M^{TT'}$ is the averaged moment of the nearest Sc neighbors (in μ_B). Only compounds containing Ni are labeled explicitly.

Therefore, the transferred hyperfine field is significantly larger in Ni compounds than in the other cases. One can approximately account for these effects by plotting $\sigma_c^{val-SCF}$ against (M^{Sc} − 0.2 $M^{TT'}$) (Figure 9), where $M^{TT'}$ stands for the average magnetic moment of the TT′ neighbors of Sc. We can also try a similar analysis for Al, where the overall $\sigma_c^{val-SCF}$ is smaller. However, we do not get such a perfect relation here since the induced Al magnetic moments are much smaller and therefore not such a good (and important) descriptor as the larger (localized) Sc moments. While the transferred hyperfine fields improve the correlation, the simple scaling with the magnitude of these moments does not hold as well. Finer details which are not taken into account in this simple analysis of the transferred hyperfine fields also matter. For example, the distance between Al (Sc) and the TT′ atoms (lattice parameter in the case of the Heusler alloys) or, more accurately, the actual overlap between Al (Sc) s-wave functions with the corresponding TT′ orbitals must be considered in a more quantitative model.

The Al shielding in the ScT_2Al series has been recently computed using the projector augmented wave (PAW) approach.[7] It is very interesting to compare directly the results obtained with the two methods. In Figure 10, we show the correlation between our APW and their PAW results, where we include all three results obtained using different projector sets as obtained in ref 7. Although the methods use a different representation of the wave functions, potential and density, both use a similar formalism for computing the orbital and spin components of the shielding; therefore, the numbers should be directly comparable. In fact, the total shifts δ correlate reasonably well between these two methods and also the PAW results do not depend too much on the chosen PAW potentials. However, this seems to come from some fortuitous error cancellation, because it is not the case for the individual orbital or spin part of the shielding (σ_o and σ_{spin} in Figure 10). For σ_o the JTH projector set produces results closest to ours for Ni, Pd, and Pt. However, for Cu and Ag, both PSL-n-n and PSLR-n-n lead to better agreement with APW. For the spin component of the shielding, JTH gives results that are closer to ours for all compounds, while for the total shielding both PSL-n-n and PSLR-n-n sets give the best agreement with our APW results (and to the experimental values as concluded in ref 7). It is unfortunate that the authors of ref 7 did not trust their Sc shieldings, since it would be very interesting to compare them to ours for this more complicated case.

DOI: 10.1021/acs.jpcc.7b03494
J. Phys. Chem. C 2017, 121, 12398−12406

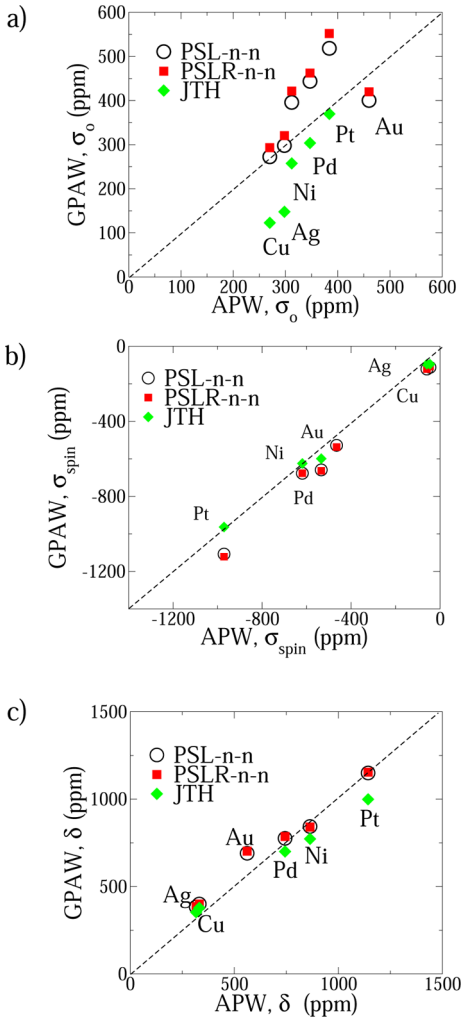

Figure 10. Comparison of Al shielding in ScT_2Al computed using our APW approach with the GIPAW results from ref 7. The (a) orbital, (b) spin, and (c) total shifts evaluated with respect to $AlPO_4$ are shown, and we have included the results obtained with three different projector sets (PSL-nn, PSLR-n-n, JTH) as given in ref 7.

CONCLUSIONS

We have presented a theoretical study of Al and Sc NMR shifts in ScTT′Al Heusler intermetallic phases. Our calculated shifts are compared to the experimental data provided in ref 8. With the exception of one single data point for ScNiAuAl, the agreement between theory and experiment for Al shifts is excellent. We could trace this difference to a problematic sample in the measurements. For Sc, however, there are three data points breaking the correlation. We have shown using a set of insulating Sc compounds that the orbital component of the shielding for Sc can be evaluated quite precisely and the discrepancy between theory and experiment does not exceed a few parts per million. Therefore, we may conclude that the lack of accuracy for the three computed Sc shieldings is probably in the spin component. It is for instance known that the calculated hyperfine field of bcc Fe is 10% too small as compared to experimental Mössbauer measurements, although the calculated magnetic moment agrees perfectly with experiment.[35] It is also known that in some cases GGA calculations overestimate magnetism[29] and better DFT approximations may be necessary in certain cases. Alternatively, experimental problems with these three samples due to nonstoichiometry or (partial) disorder could also cause the discrepancies.

Our results indicate that, in order to correctly compute the spin part of the response to an external magnetic field, self-consistency effects for all states, including the low lying core, have to be considered carefully. As presented for both Al and Sc, the paramagnetic spin polarization around the Fermi level leads to large perturbations of the potential that polarizes core, semicore, and valence states. In the case of Sc the large induced 3d moment results in a very large core polarization with opposite spin and leads to very small Knight shifts. This leads in the end to the surprising fact that the Sc NMR shifts in these intermetallic phases are completely dominated by the chemical shift and the effect of the Knight shift (spin contribution) is almost negligible.

We also compared our computed Al shieldings to recently published results obtained with the PAW approach, where they tested three different potentials (projectors). Interestingly, we find that our total shieldings agree reasonably well with the PAW calculations, but the individual orbital and spin terms do not. Sometimes one or the other PAW potential gives better or worse agreement, but the errors seem to cancel to some extent.

AUTHOR INFORMATION

Corresponding Author

*E-mail: rolask@ihpc.a-star.edu.sg.

ORCID

Khoong Hong Khoo: 0000-0002-4628-1202

Robert Laskowski: 0000-0001-7311-7582

Notes

The authors declare no competing financial interest.

ACKNOWLEDGMENTS

The authors gratefully acknowledge the use of computational resources at the A*STAR Computational Resource Center and National Supercomputing Center Singapore. P.B. acknowledges support by the Austrian Science Foundation FWF, Project F41 (SFB-Vicom).

REFERENCES

(1) Kohn, W.; Sham, L. J. Self-Consistent Equations Including Exchange and Correlation Effects. *Phys. Rev.* **1965**, *140*, A1133−A1138.

(2) Hohenberg, P.; Kohn, W. Inhomogeneous Electron Gas. *Phys. Rev.* **1964**, *136*, B864−B871.

(3) Mauri, F.; Pfrommer, B. G.; Louie, S. G. Ab Initio Theory of NMR Chemical Shifts in Solids and Liquids. *Phys. Rev. Lett.* **1996**, *77*, 5300−5303.

(4) Pickard, C. J.; Mauri, F. All-Electron Magnetic Response with Pseudopotentials: NMR Chemical Shifts. *Phys. Rev. B: Condens. Matter Mater. Phys.* **2001**, *63*, 245101.

(5) Laskowski, R.; Blaha, P. NMR Shielding in Metals Using the Augmented Plane Wave Method. *J. Phys. Chem. C* **2015**, *119*, 19390−19396.

(6) Laskowski, R.; Khoo, K. H.; Haarmann, F.; Blaha, P. Computational Study of Ga NMR Shielding in Metallic Gallides. *J. Phys. Chem. C* **2017**, *121*, 753−760.

(7) Ferreira, A. R.; Reuter, K.; Scheurer, C. Toward Routine Gauge-Including Projector Augmented-Wave Calculations for Metallic Systems: The Case of ScT2Al (T = Ni, Pd, Pt, Cu, Ag, Au) Heusler Phases. *J. Phys. Chem. C* **2016**, *120*, 25530−25540.

(8) Benndorf, C.; Niehaus, O.; Eckert, H.; Janka, O. 27Al and 45Sc NMR Spectroscopy on ScT2Al and Sc(T0.5T′0.5)2Al (T = T′ = Ni,

DOI: 10.1021/acs.jpcc.7b03494
J. Phys. Chem. C 2017, 121, 12398−12406

Pd, Pt, Cu, Ag, Au) Heusler Phases and Superconductivity in Sc(Pd0.5Au0.5)2Al. *Z. Anorg. Allg. Chem.* **2015**, *641*, 168−175.
(9) Graf, T.; Felser, C.; Parkin, S. S. P. Simple Rules for the Understanding of Heusler Compounds. *Prog. Solid State Chem.* **2011**, *39*, 1−50.
(10) Felser, C.; Wollmann, L.; Chadov, S.; Fecher, G. H.; Parkin, S. S. P. Basics and Prospective of Magnetic Heusler Compounds. *APL Mater.* **2015**, *3*, 041518.
(11) Felser, C.; Fecher, G.; Balke, B. Spintronik: Eine Herausforderung für Materialwissenschaften und Festkörperchemie. *Angew. Chem.* **2007**, *119*, 680−713.
(12) Chen, S.; Ren, Z. Recent Progress of Half-Heusler for Moderate Temperature Thermoelectric Applications. *Mater. Today* **2013**, *16*, 387−395.
(13) Winterlik, J.; Fecher, G. H.; Thomas, A.; Felser, C. Superconductivity in Palladium-Based Heusler Compounds. *Phys. Rev. B: Condens. Matter Mater. Phys.* **2009**, *79*, 064508.
(14) Abragam, A. *Principles of Nuclear Magnetism*; Oxford University Press: Oxford, U.K., 1961.
(15) Slichter, C. P. *Principles of Magnetic Resonance*, 3rd ed.; Springer-Verlag: Berlin, 1990.
(16) Knight, W. D.; Kobayashi, S. Knight Shift. In *Encyclopedia of Nuclear Magnetic Resonance*; Grant, D. M., Harris, R. K., Eds.; John Wiley & Sons: Chichester, U.K., 1996; pp 2672−2679.
(17) Knight, W. D.; Kobayashi, S.-I. Knight Shift. In *Enzyclopedia of Magnetic Resonance*; Harris, R. K., Wasylishen, R. E., Eds.; John Wiley: Chichester, U.K., 2007.
(18) Haarmann, F. Quadrupolar NMR of Intermetallic Compounds. In *Encyclopedia of Magnetic Resonance*; Harris, R. K., Wasylishen, R. E., Duer, M. J., Eds.; John Wiley: Chichester, U.K., 2011.
(19) Yates, J. R.; Pickard, C. J.; Mauri, F. Calculation of NMR Chemical Shifts for Extended Systems Using Ultrasoft Pseudopotentials. *Phys. Rev. B: Condens. Matter Mater. Phys.* **2007**, *76*, 024401.
(20) Singh, D. J.; Nordström, L. *Planewaves, Pseudopotentials and the LAPW Method*, 2nd ed.; Springer: New York, 2006.
(21) Blaha, P.; Schwarz, K.; Madsen, G. K. H.; Kvasnicka, D.; Luitz, J. *WIEN2k, An Augmented Plane Wave Plus Local Orbitals Program for Calculating Crystal Properties*; Vienna University of Technology: 2001.
(22) Laskowski, R.; Blaha, P. Calculations of NMR Chemical Shifts with APW-Based Methods. *Phys. Rev. B: Condens. Matter Mater. Phys.* **2012**, *85*, 035132.
(23) Laskowski, R.; Blaha, P. Calculating NMR Chemical Shifts Using the Augmented Plane-Wave Method. *Phys. Rev. B: Condens. Matter Mater. Phys.* **2014**, *89*, 014402.
(24) Gregor, T.; Mauri, F.; Car, R. A Comparison of Methods for the Calculation of NMR Chemical Shifts. *J. Chem. Phys.* **1999**, *111*, 1815−1822.
(25) Blügel, S.; Akai, H.; Zeller, R.; Dederichs, P. H. Hyperfine Fields of 3*d* and 4*d* Impurities in Nickel. *Phys. Rev. B: Condens. Matter Mater. Phys.* **1987**, *35*, 3271−3283.
(26) d'Avezac, M.; Marzari, N.; Mauri, F. Spin and Orbital Magnetic Response in Metals: Susceptibility and NMR Shifts. *Phys. Rev. B: Condens. Matter Mater. Phys.* **2007**, *76*, 165122.
(27) Perdew, J. P.; Burke, K.; Ernzerhof, M. Generalized Gradient Approximation Made Simple. *Phys. Rev. Lett.* **1996**, *77*, 3865−3868.
(28) Bräuniger, T.; Hofmann, A. J.; Moudrakovski, I. L.; Hoch, C.; Schnick, W. A 45Sc-NMR and DFT Calculation Study of Crystalline Scandium Compounds. *Solid State Sci.* **2016**, *51*, 1−7.
(29) Singh, D.; Ashkenazi, J. Magnetism with Generalized-Gradient-Approximation Density Functionals. *Phys. Rev. B: Condens. Matter Mater. Phys.* **1992**, *46*, 11570.
(30) Ortenzi, L.; Mazin, I.; Blaha, P.; Boeri, L. Accounting for Spin Fluctuations Beyond Local Spin Density Approximation in the Density Functional Theory. *Phys. Rev. B: Condens. Matter Mater. Phys.* **2012**, *86*, 064437.
(31) Laskowski, R.; Blaha, P. Origin of NMR Shielding in Fluorides. *Phys. Rev. B: Condens. Matter Mater. Phys.* **2012**, *85*, 245117.
(32) Laskowski, R.; Blaha, P. Understanding of 33S NMR Shielding in Inorganic Sulfides and Sulfates. *J. Phys. Chem. C* **2015**, *119*, 731−740.
(33) Dubiel, S. Relationship Between the Magnetic Hyperfine Field and the Magnetic Moment. *J. Alloys Compd.* **2009**, *488*, 18−22.
(34) Akai, H.; Akai, M.; Blügel, S.; Zeller, R.; Dedetichs, P. Hyperfine Fields of Impurities in Ferromagnets. *J. Magn. Magn. Mater.* **1984**, *45*, 291−297.
(35) Novak, P.; Chlan, V. Contact Hyperfine Field at Fe Nuclei from Density Functional Calculations. *Phys. Rev. B: Condens. Matter Mater. Phys.* **2010**, *81*, 174412.

DOI: 10.1021/acs.jpcc.7b03494
J. Phys. Chem. C 2017, 121, 12398−12406